Development of the Detecting System for Steel Plate with Backside Defect Using an Array of AMR Sensor

Koji Morita, Keishu Shiga, Yuta Haga, Kenji Sakai, Toshihiko Kiwa, Keiji Tsukada
Graduate School of Natural Science and Technology, Okayama University
Okayama, Japan
e-mail: (en422454, pcf45clo, pgtw6b5j)@s.okayama-u.ac.jp
(sakai-k, kiwa, tsukada)@cc.okayama-u.ac.jp

***Abstract*—Demand for detecting deep defects in the steel plate is increasing. We have reported a magnetic flux leakage testing (MFLT) system to detect deep defects and create magnetic imaging methods that indicate the backside defect. However, the developed system with one magnetic sensor requires XY automatic positioning stage and long measurement time. In this study, to realize fast measurement for practical use, we have developed a new system which can detect the magnetic field at several measurement points simultaneously using a multi-sensor array. Using the developed system, backside corrosion of steel plates having different depth was measured and two-dimensional images were created. The detected vector signal was analyzed by adjusting phase data. As a result, the developed MFLT system showed good performance of detection limit more than 7.2 mm in depth.**

Keywords- magnetic flux leakage; magnetic imaging; AMR device; low-frequency field; backside defect

I. INTRODUCTION

Defects or refuge of steel structure, such as infrastructure, bridge legs, power plants, and heavy industry pipeline cause serious accidents. As the decrepit infrastructures are now increasing, it is very important to use non-destructive testing for detecting defects as early as possible. Generally, it is difficult to detect the defects which exist in the internal or on the backside of the steel plate. Therefore, the detection method is required to detect deep defects. In the past, various types of non-destructive testing methods have been investigated such as radiographic testing [1], ultrasonic testing [2], magnetic flux leakage testing (MFLT) [3]-[8], and eddy current testing (ECT) [9]. Ultrasonic testing is affected by the surface state of measurement sample, and it is needed to contact material for testing. Radiographic testing is dangerous for using radiation, thus it needs expert to use. From the above situation, the detecting method that is easy operation and safe is desired. MFLT and ECT testing use magnetic phenomenon, thus, these methods enable contactless, easy operation and safe measurement. MFLT is applied to ferromagnetic material, such as steel and it is a method to detect a magnetic flux from the sample's surface which leaked at defects due to differences in permeability when an external magnetic field is applied to the sample. Although the conventional MFLT system is generally used for surface inspection [10], considering practice use, it is demanded that the detection of deep defect or backside defect. Therefore, we reported a two-dimensional mapping system for backside defects of a steel plate using MFLT. However, the system consisting of one channel magnetic sensor required two-dimensional stage to obtain the two-dimensional magnetic field mapping and long measurement time. In this study, we have developed a new system which can measure several magnetic signals simultaneously using a multi-sensor array was developed for rapid measurement.

Section II describes the detailed description about system configuration of the developed system. Section III describes the scheme of the experiment and the sample we used. Section IV describes the performance of the developed system was compared with the previous system measuring the steel plate with corrosion. Section V describes the conclusion.

II. DEVELOPED SYSTEM

Figure 1 shows the developed MFLT system. The MFLT system consists of a probe using an 8 channel AMR sensor array and a half-shaped yoke, a pair of excitation coil at both ends of the yoke, preamplifiers, a lock-in amplifier for phase sensitive detection (PSD), a current source, an oscillator, and a PC. Each AMR sensor is located between the both of ends of the yoke, and the interval of sensor is 10 mm. The liftoff between AMR sensor and sample surface was 1 mm. AMR sensors detect the y-axis component of the magnetic field which is parallel to both yoke ends, as shown in Figure 1. The current source applies an electrical current to a pair of induction coil with 25 turns connected to both ends of the yoke. AC magnetic field was induced in the sample between both ends of yoke. The induction coils were operated by sinusoidal wave of 2.5 A from the current source. Using a magnetic field of low frequency, eddy current can be ignored because the skin depth increases with increasing frequency. Thus, the detected magnetic field was mainly due to the magnetic leakage under the operating condition. The yoke is 10 pieces of non-oriented electromagnetic steel plate.

Figure 2 shows the previous MFLT system. The main difference between developed system and previous system is the length of the yoke. The probe consists of a half-shaped short yoke whose section is 10 mm × 10 mm and the induction coils at both ends of the yoke with 30

Copyright (c) IARIA, 2015. ISBN: 978-1-61208-426-8

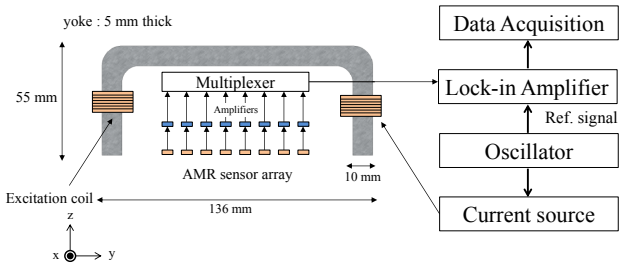

Figure 1. Schematic diagram of the developed MFLT system.

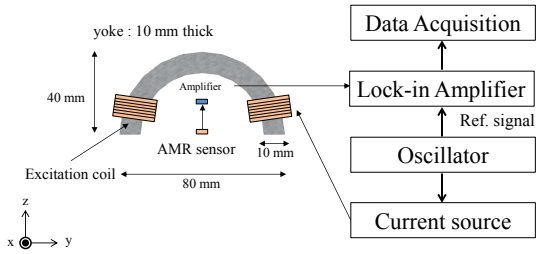

Figure 2. Schematic diagram of the previous MFLT system.

turns. The induction coils were operated by sinusoidal wave of 0.7 A from the current source. The sensor was placed 1 mm away from the sample surface. Both probes are fixed in acrylic case of nonmagnetic material not to affect the AMR sensors.

III. EXPERIMENT

The measurement samples are SS400 steel plates of 12 mm thickness which have different depth of a backside corrosion. The plate had a galvanic corrosion at the center of the plate on the backside. The state of corrosion is shown in Figure 3 and Table 1 shows the detail of the corrosion size of samples.

In the developed system, one line measurement enables multi point measurement. Therefore, the magnetic field was measured in the range of 80 mm × 150 mm around the corrosion, as shown in Figure 4. For the comparison, one line measurement was executed using the previously developed system, and the measurement point was shown as white point in Figure 4.

The magnetic flux leakage generated from the backside corrosion was detected on the front surface by AMR sensors. The interval of measurement point was 10 mm and the y-axis component of the magnetic field was measured in each system.

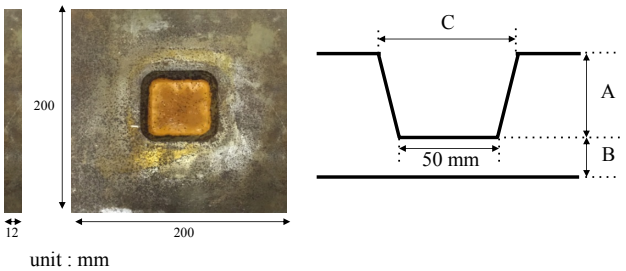

Figure 3. Test plates with corrosion.

TABLE I. THE CORROSION CONDITION OF THE TEST PLATES.

corrosion rates	10 %	20 %	40 %	50 %	60%	80 %
A : depth (mm)	1.2	2.4	4.8	6.0	7.2	9.6
B : depth from surface (mm)	10.8	9.6	7.2	6.0	4.8	2.4
C : Range of corrosion (mm)	59.0	62.05	60.12	62.07	63.89	74.0

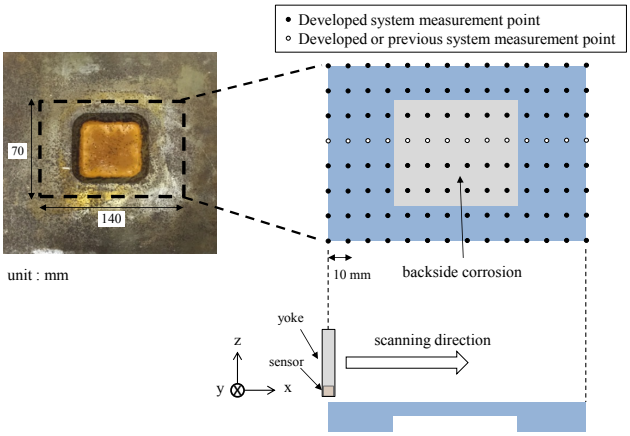

Figure 4. Measurement points for backside corrosion.

The outputs of AMR sensor were measured using a lock-in amplifier to detect the signal intensity and phase, which were synchronized with the oscillator. Overall conditions were adopted for each appropriate condition. Each probe was maintained 1 mm air gap between the yoke heads and the sample. Keeping the constant air gap between the yoke and the sample has an advantage in reproducibility compared with the direct contact method because of the non-smoothness of the sample surface due to oxidization and so on.

At each measurement point, signal intensity and phase was measured. Using the intensity $M_{mes,i}$ and phase α_i, the imaginary part of the signal with the common phase θ is calculated as follows [11].

$$M_{img} = |M_{mes,i}| \times \sin(\alpha_i + \theta) \quad (1)$$

The θ is adjusting phase which adjust shifted phase caused by the system phase shift and the θ depends on the system configuration. Thus, if an optimum θ is obtained by measuring a standard sample, adjustment of θ is not required in other measurement.

IV. RESULTS AND DISCUSSIONS

A. Basic Characteristics of Developed Sensor Array System

Figure 5 and 6 show each system outputs curves for some common phase θ obtained by measurements on the steel plate with corrosion rate of 80 % using 10 Hz sine wave current. The data of Figure 5 is fifth sensor (channel 5) and this is the same position as that of the previous system. Comparing both results, each system can detect the magnetic flux leakage caused by the backside corrosion with the common phase $\theta = 0$ degrees. The previous

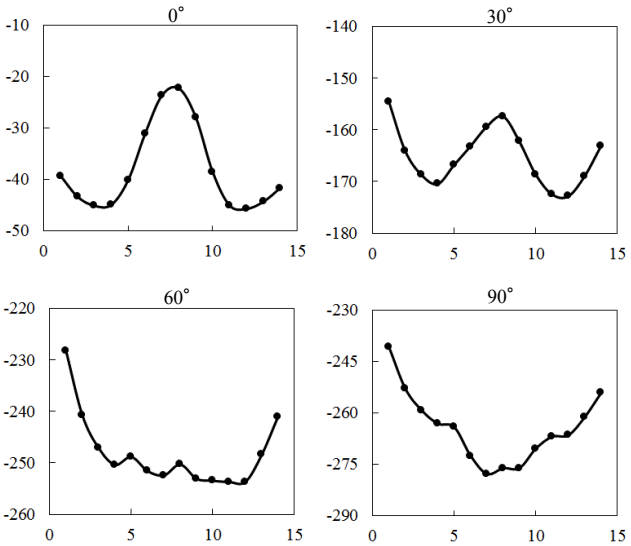

Figure 5. Magnetic flux leakage data with different phase of developed system using multi-sensor array.

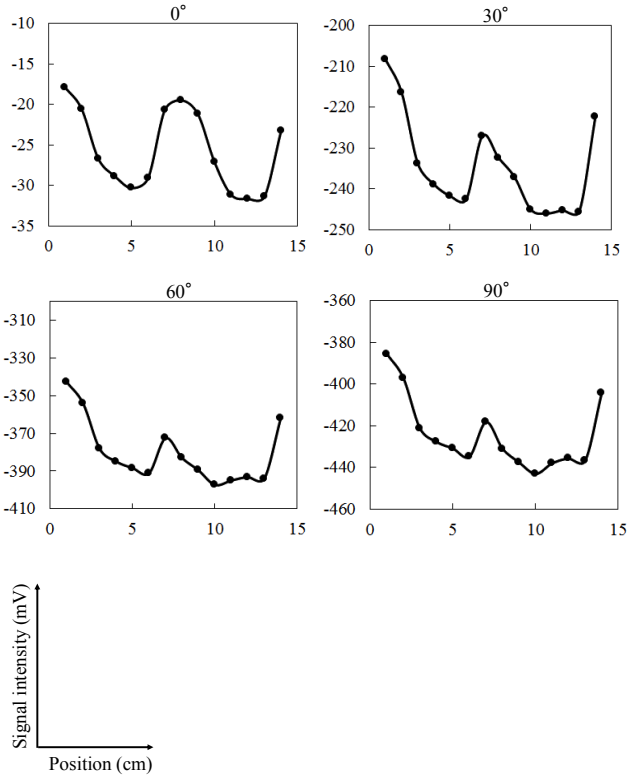

Figure 6. Magnetic flux leakage with different phase of the previous system using one sensor.

system can detect the backside corrosion using above condition. From this result, it was found that the signal changes detected by the developed system are correlated to the backside corrosion. Even if a long yoke was used for applying a magnetic field, the backside corrosion could be curves shown in Figure 5 and 6 showed the same tendency. This means using long yoke enables to detect the magnetic flux leakage using a sensor array. Thus, a measurement system which can realize simultaneous measurement of multi lines is possible by only carrying out one line measurement using a sensor array.

However, the magnetic field generated by a long yoke was not constant at each position of AMR sensor. Figure 7 shows the magnetic field distribution between the ends of the yoke in the air under the condition that the excitation coil was operated by a current of 10 Hz and 2.5 A sine wave. The magnetic signal was detected by each sensor. The magnetic signal intensity became large and the phase shift was small near by the ends of the yoke. In this condition, the magnetic image created by multi point measurement is affected by the distribution of the magnetic field. Therefore, in this measurement, to reduce the influence of distribution of the magnetic field, the reference signal vector measured with non-defect sample was subtracted from the measured signal vector with defect sample. The measurement point of reference signal was the center line of the non-defected samples. After that, the magnetic images calculated from the sbtructed signal vector using (1). Figure 8 shows the magnetic image before subtracting the reference signal (a), and after subtracting the reference signal (b). The corrosion rate is 80 %. Comparing Figure 8 (a) with Figure 8 (b), the influence of the distribution of the magnetic field was reduced by subtracting the signal of non-defect sample, and a clear magnetic image that shows corrosion could be obtained.

B. System Optimization

To optimize the system, the appropriate frequency and common phase using 60 % corrosion rate sample was examined. Figure 9 shows magnetic images using a 5 Hz excitation frequency and various common phases and Figure 10 shows that using a 10 Hz and various common phases. Magnetic images with a common phase 0° showed the clearest corrosion image, and magnetic images with 5 Hz shows the presence of the backside corrosion more clearly than that of 10 Hz. This means that the magnetic

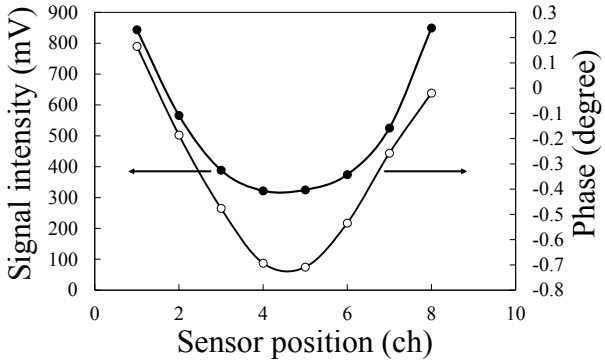

Figure 7. The signal intensity and phase of each sensor caused by the distribution of the magnetic field.

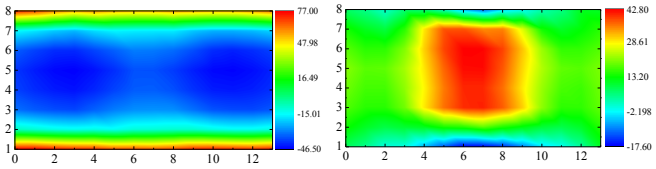

(a) (b)

Figure 8. The magnetic images affected with the distribution of the magnetic field (a) and calculated image (b).

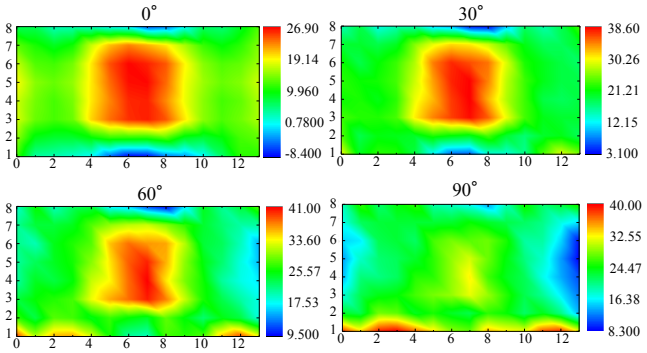

Figure 9. Magnetic images with 5 Hz and different phase.

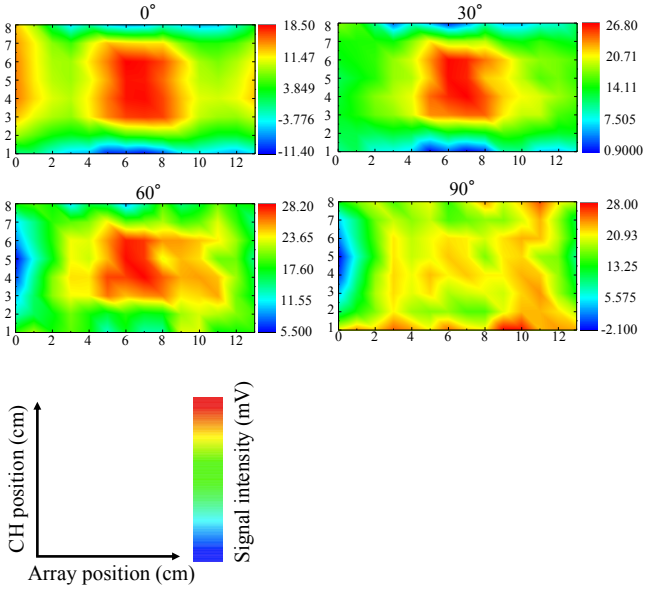

Figure 10. Magnetic images with 10 Hz and different phase.

field penetrated inside the steel plate increased with decreasing the frequency due to the skin effect, and the depth of penetrated magnetic signal with 10 Hz decreased compared to that with 5 Hz. Therefore, the optimum condition was determined as the frequency is 5 Hz and common phase is 0°.

C. *Evaluation of Depth Profile*

To evaluate the developed system under the optimum condition, we measured magnetic images using the steel plates which have different corrosion rate. The excitation coils were operated with 5 Hz and 2.5 A sine wave from a current source and the common phase was 0°. For all samples, one line measurement was performed and magnetic signal was measured by 8 sensors. Using the detected magnetic signals, the magnetic images of the samples with different corrosion rates of 10, 20, 40, 50, 60, and 80 % were obtained.

Figure 11 shows the result of magnetic images. The images show the existence of the corrosion and it becomes clear with increasing the actual corrosion rate of more than 40%. On the other hand, the magnetic images with the corrosion rate of 10 and 20 % show unclear images. These unclear images derived from that the magnetic flux leakage did not leak enough when the magnetic field was applied at the sample with low corrosion, and the difference of signal intensity between corrosion part and healthy part was small.

Next, we examined to evaluate the relation between the change of the magnetic field intensity and corrosion rates quantitatively. The change of the magnetic field which is along the dotted line in the Figure 12 (a) is shown in Figure 12 (b). The changes of each corrosion rate of 10, 20, 40, 50, 60, and 80% are shown. The ΔB is defined as the subtracted value between the maximum and minimum values for each sample as shown in Figure 12 (b). The value of ΔB increased according to the increase of the corrosion rates. Comparing ΔB with the magnetic image of 10, 20 %, the magnetic images are unclear and the change of the ΔB for 10 % and 20 % changed little. Therefore, more than 40 % corrosion rate can be detected using the developed system. This corresponds to the depth of approximately 7.2 mm from the surface of the front. Figure 13 shows the relation between the depth of defect and ΔB. The ΔB was chosen thinning rate are 80, 60, 50, 40 % which are ΔB clearly changes. ΔB decreased with the increment of the depth of the defect. Using the magnetic image and ΔB, we can survey the backside defect's size and depth.

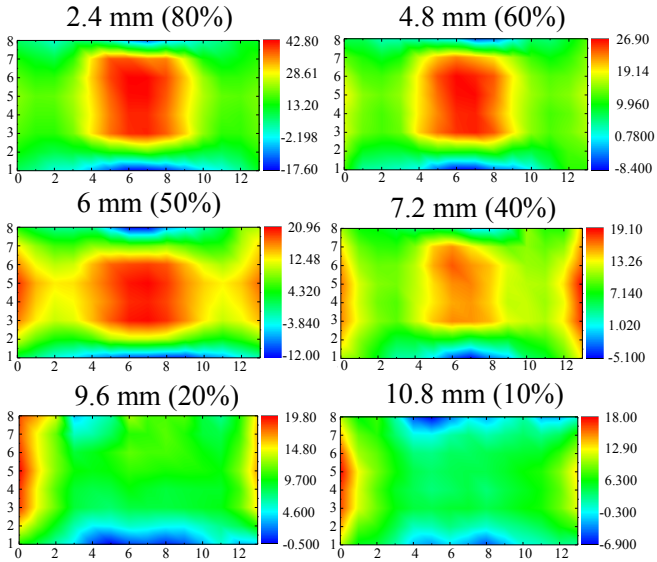

Figure 11. Magnetic images of corrosion with different wall thinning rate.

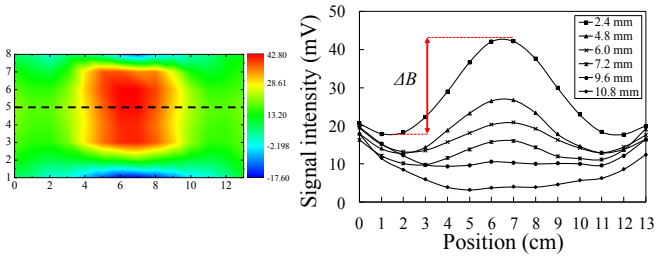

Figure 12. Example of the extracted line (a) and the definition of ΔB (b).

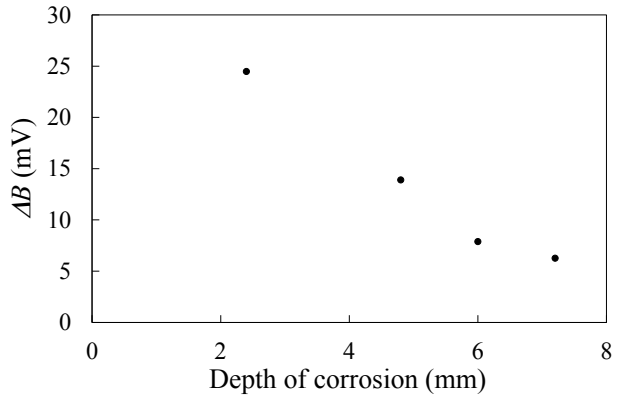

Figure 13. Relationship of the depth of defect and ΔB.

To improve detecting ability for deep corrosion, it is required to gain the enough magnetic flux leakage due to the backside corrosion by increasing the applied magnetic field. To realize this, appressing the sensor probe to a steel plate will be effective to reduce the dispersion of the magnetic flux leakage signals which is derived from the fluctuation of lift-off and leakage of the magnetic flux to the outside.

V. CONCLUSIONS

A new MFLT system with a multi-sensor array for practical use was developed. Arraying the sensors enabled reducing positioning time to settle the sensor probe and sensors, and the system enabled rapid detection of backside defect. When the magnetic field of low frequency was applied, it was possible to detect the deepest defect. In addition, the stronger magnetic field could detect the deep defect. Under these optimized conditions, the developed system showed good detection limit more than 7.2 mm in depth.

REFERENCES

[1] I. G. Kazantsev, I. Lemahieu, G. I. Salov, and R. Denys, "Statistical detection of defects in radiographic images in nondestructive testing," Signal Processing, vol. 82, issue 5, May 2002, pp. 791-801.

[2] M. Kharrat and L. Gaillet, "Non-destructive evaluation of anchorage zones by ultrasonics techniques," Ultrasonics, Available online 23 March 2015.vol. 61, August 2015, pp. 52-61.

[3] T. Bubenik, "Electromagnetic methods for detecting corrosion in underground pipelines: magnetic flux leakage (MFL)," In Underground Pipeline Corrosion, Woodhead Publishing, 2014, pp. 215-226.

[4] M. M. Tehranchi, S. M. Hamidi, H. Eftekhari, M. Karbaschi, and M. Ranjbaran, "The inspection of magnetic flux leakage from metal surface cracks by magneto-optical sensors," Sensors and Actuators A: Physical, vol. 172, issue 2, December 2011, pp. 365-368.

[5] Y. Zhang, Z. Ye, and C. Wang, "A fast method for rectangular crack sizes reconstruction in magnetic flux leakage testing," NDT & E International, vol. 42, issue 5, July 2009, pp. 369-375.

[6] R. Baskaran and M. P. Janawadkar, "Imaging defects with reduced space inversion of magnetic flux leakage fields," NDT & E International, vol. 40, Issue 6, September 2007, pp. 451-454.

[7] J. Atzlesberger and B. Zagar, "Magnetic flux leakage measurement setup for defect detection," Procedia Engineering, vol. 5, 2010, pp. 1401-1404.

[8] P. Wang, Y. Gao, G. Tian, and H. Wang, "Velocity effect analysis of dynamic magnetization in high speed magnetic flux leakage inspection," NDT & E International, vol. 64, June 2014, pp. 7-12.

[9] D. F. He, M. Shiwa, J. P. Jia, J. Takatsubo, and S. Moriya, "Multi-frequency ECT with AMR sensor," NDT & E International, vol. 44, issue 5, September 2011, pp. 438-441.

[10] M. M. Tehranchi, M. Ranjbaran, and H. Eftekhari, "Double core giant magneto-impedance sensors for the inspection of magnetic flux leakage from metal surface cracks," Sensors and Actuators A: Physical, vol. 170, issues 1–2, November 2011, pp. 55-61.

[11] K. Tsukada, M. Yoshioka, Y. Kawasaki, and T. Kiwa. "Detection of back-side pit on a ferrous plate by magnetic flux leakage method with analyzing magnetic field vector," NDT&E International vol. 43, issue 4, June 2010, pp.232-328.

Copyright (c) IARIA, 2015. ISBN: 978-1-61208-426-8